A Microfabricated Spiral-Groove Turbopump Supported on Microball Bearings

Christopher Mike Waits, *Student Member, IEEE*, Matthew McCarthy, and Reza Ghodssi, *Member, IEEE*

***Abstract*—The development of a microfabricated turbopump that is capable of delivering liquid fuel with the flow rates and pressures required for portable power generation is reported. The device is composed of a spiral-groove viscous pump driven by a radial in-flow microturbine and supported using a newly developed encapsulated microball bearing. A planar-contact bearing raceway is employed using 285-μm-diameter 440C stainless steel microballs. A modification to the raceway geometry, as compared to previous designs, has enabled repeatable operation of the microturbine at speeds up to 87 000 r/min, showing negligible variations in performance for over 6 h and 3.8 million revolutions. Pumping has been demonstrated with water as the working fluid for flow rates of 10–80 mL/h and pressures rises of up to 8.2 kPa. This is the first application to incorporate an encapsulated microball bearing support mechanism, to achieve rotational speeds in excess of 50 000 r/min using a contact bearing, and to demonstrate reliable operation of more than 1 million revolutions. [2009-0123]**

***Index Terms*—Microelectromechanical systems (MEMS) bearings, micropumps, microturbines, power MEMS, turbopump.**

I. INTRODUCTION

SINCE the mid-1990s, power microelectromechanical systems (PowerMEMS) components and systems have received increased attention for portable (< 100-W) power applications. For these applications, liquid hydrocarbon fuels are favorable energy sources compared to conventional battery chemistries due to the significant energy density and power density contained within the fuel (at only 10% efficiency, diesel fuel can yield 4.2 MJ/kg, which is ten times more than 0.36 MJ/kg for primary batteries). PowerMEMS devices that have been investigated for portable power and take advantage of the high density energy stored in hydrocarbons include the following: gas turbine generators [1]–[3], steam engine generators [4], rotary engine generators [5], and fuel cells [6], [7], to name a few.

Compact solutions for pumping liquid fuels are highly sought after in the miniaturized heat engine and fuel cell technologies being developed. Compact liquid pumps with form factors below 1 cm^3, flow rates in the range of 10–100 mL/h, and pressure capabilities in the range of 5–10 kPa would enable a higher level of performance and compactness but are not currently commercially available. Numerous MEMS-based pumping mechanisms have been demonstrated, of which reviews can be found in [8] and [9]. Pumping technologies designed for a variety of liquid fuels require flexibility because of the varying fluid properties, and as such, the pumping mechanism cannot be based solely on the electrical, magnetic, or pH properties. Based on this requirement, purely mechanical pumping mechanisms that depend only on the viscosity and density of the fluid are best suited for multifuel-type delivery applications.

Positive displacement pumps have dominated MEMS-based mechanical pump research with typical configurations using a pulsed diaphragm to provide flow between two opposing valves [9]. Flow rates in the range of microliters per minute to milliliters per minute have been demonstrated using batch microfabrication, but those with a form factor below 1 cm^3 have been limited to low flow rates, typically liquid flow rates below 60 mL/h for the pressure range of interest. Additional drawbacks of positive displacement pumps are rectification for low-frequency operation and the requirement of valves; these are additional moving components that impact both the lifetime and reliability of the pump device.

Alternative to MEMS displacement pumping mechanisms, rotational-based continuous pumping mechanisms that are capable of achieving the required pressures and flow rates have been demonstrated [10]–[12]. In most cases, these mechanisms operate via a rotor driven by an external or an integrated motor. Blanchard *et al.* [10] used a flat disc attached to a shaft and driven externally via a brushless dc motor in combination with a C-shaped channel positioned below the disc to demonstrate 0–285 mL/h with a pressure range of 0–31.1 kPa. Two groups have also demonstrated rotational-based pumps that use integrated radial in-flow microturbines. Deux [11] demonstrated a 200-mL/h JP-8 flow rate with up to 14-kPa pressure using a radial in-flow microturbine integrated with a centrifugal geometry and operating at speeds up to 300 000 r/min. Lee *et al.* [12] demonstrated a 36-mL/h water flow rate with a maximum pressure of 207 kPa using a spiral-groove turbopump with a cascaded radial in-flow microturbine running at speeds of 120 000 r/min. Both groups used hydrostatic air bearings to support the rotors. Although this approach allows for significant rotational speeds, the fabrication is complex, and the operation requires externally controlled pressure plenums with up to 586-kPa pressures [11]. So far, widespread use of rotational-based pump technologies has been limited primarily due to the need for external motors or externally controlled bearing mechanisms. In this paper, microball bearings are integrated

Manuscript received May 8, 2009; revised October 19, 2009. First published December 1, 2009; current version published February 3, 2010. This work was supported in part by the Sensors and Electron Devices Directorate, U.S. Army Research Laboratory, under the Cooperative Agreement W911NF0520026. Subject Editor Y. Zohar.

C. M. Waits is with the Sensors and Electron Devices Directorate, U.S. Army Research Laboratory, Adelphi, MD 20783 USA (e-mail: cwaits@arl.army.mil).

M. McCarthy is with the Department of Mechanical Engineering, Massachusetts Institute of Technology, Cambridge, MA 02139 USA.

R. Ghodssi is with the MEMS Sensors and Actuators Laboratory, Department of Electrical and Computer Engineering, Institute for Systems Research, University of Maryland, College Park, MD 20742 USA.

Digital Object Identifier 10.1109/JMEMS.2009.2035525

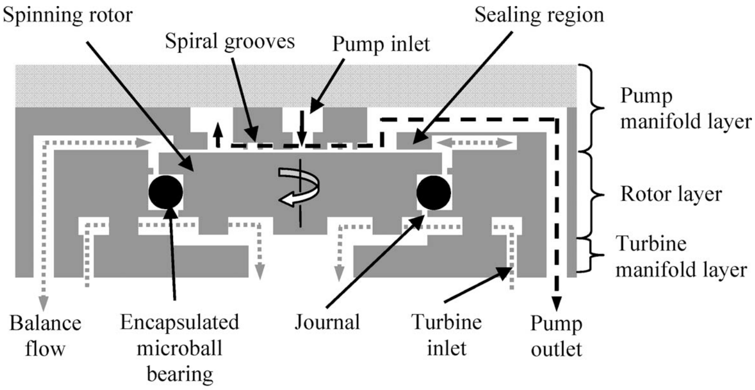

(a) **Turbopump**

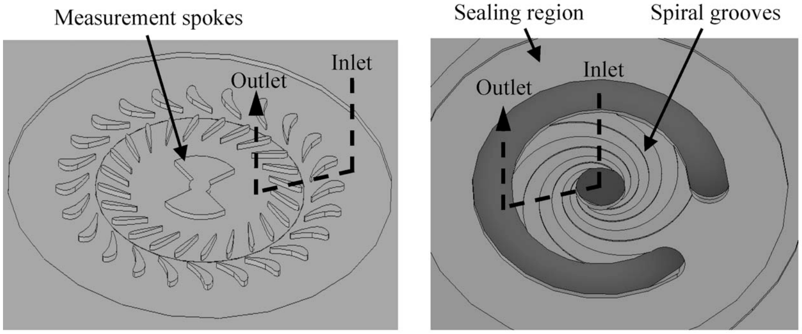

(b) **Microturbine** (c) **Spiral-Groove Pump**

Fig. 1. Drawings of the spiral-groove turbopump showing (a) the device cross section, (b) the radial in-flow air turbine, and (c) the spiral-groove pump region and seal.

with a radial in-flow air turbine to eliminate the need for an external motor or bearing control mechanism. Furthermore, the fabrication complexity of microball bearings is simplified when compared to air bearings and can be readily integrated with a motoring mechanism.

Our research group has pioneered the development of ball bearing support mechanisms for silicon micromachines and demonstrated a continuous evolution of the technology for low-friction supports [13]–[15]. In previous work, an encapsulation technique was demonstrated using a high-wear point-contact design that enabled complete integration of a microball bearing and provided full support to a spinning rotor [16], [17]. Following this, a planar-contact design was implemented in a radial in-flow microturbine platform, demonstrating reduced wear and allowing the development of an empirical model for bearing friction [18]–[20]. The microturbine platform was the first demonstration of a high-speed low-wear microball-bearing-supported device showing repeatable operation up to 10 000 r/min in air. However, the microball raceway had a critical design flaw, making it inadequate for long-term operation and requiring a long burn-in period with multiple cleaning steps due to the generation of wear debris.

In this paper, a new spiral-groove viscous pump is integrated with the previously developed radial in-flow microturbine and microball bearing platform to demonstrate a microfabricated turbopump that is implemented on a single platform. The turbopump was designed for liquid fuel delivery applications that meet the requirements of flow rate and pressure in portable power applications. Furthermore, the microball bearing raceway was modified from previously reported designs in [18]–[20] to improve both reliability and performance.

II. DEVICE DESIGN

A. *Turbopump Overview*

The microfabricated turbopump is composed of three key components: a spiral-groove viscous pump, an encapsulated microball bearing, and a radial in-flow microturbine. These components are integrated together within the pump manifold layer, the rotor layer, and the turbine manifold layer as shown in Fig. 1. The turbopump is operated by spinning the rotor using the microturbine shown in Fig. 1(b). The microball bearings support the rotor in the radial direction and prevent the turbine blades from rubbing on the lower turbine manifold surface in the thrust direction. The topside of the spinning rotor is a flat surface in close proximity to static spiral grooves on the pump manifold layer [Fig. 1(c)], thus creating a small pump gap between the two layers. Viscous forces within the pump gap cause the liquid to be dragged when the rotor is spinning while the spiral grooves guide the flow radially outward. The liquid within the pump is prevented from leaking into the bearings and out of the device using a pressure seal between a nitrogen balance channel and the liquid at the pump outlet [Fig. 1(a)].

B. *Microturbine*

A radial in-flow microturbine was incorporated with the pump and bearing structures as an actuation mechanism and

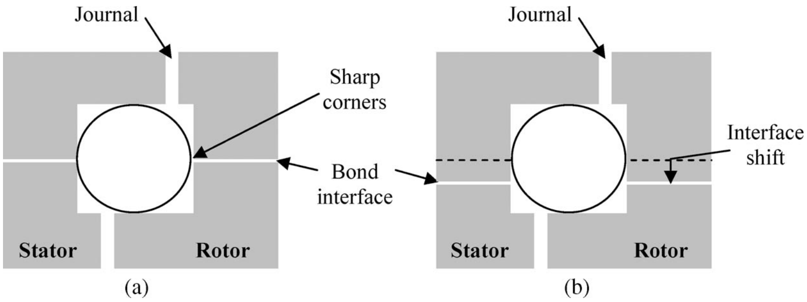

Fig. 2. Schematic drawings of the planar-contact bearing where (a) shows the previous raceway design [20] and (b) shows the current current design.

is shown in Fig. 1(b). To operate the turbine, flow is passed through 24 inlet orifices on the turbine manifold layer, through 29 stator vanes and 24 rotor blades on the rotor layer, before exiting through a hole on the turbine manifold layer located just below the rotor center. The design of the microturbine used in this paper can be found in [20]. The turbine was designed for a speed of 100 000 r/min at a flow rate of 6 slm and 0.5 W of mechanical power. The rotor diameter was kept in this paper to be 10 mm, and the blade height was made to be 200 μm to provide sufficient torque at low turbine flow rates.

C. Encapsulated Microball Bearing

The encapsulated microball bearing shown in Fig. 1(a) within the rotor layer was designed in the same manner as our previous work, which characterized the radial in-flow microturbine and microball bearing mechanism [18]–[20]. The bearing is encased by two bonded silicon layers with a raceway etched into each layer. A journal is etched completely through each wafer to create a rotor that is only supported by the microball bearings. In our previous work, the bond interface between the two raceway layers was designed at the center and inside the microball wear track as shown in Fig. 2(a). The free edges at the bond interface created stress concentrations that led to excessive wearing and chipping and thereby increased the friction within the microball bearing and decreased the turbine performance over time. Subsequently, cleaning was required to restore the operation back to peak performance. In this paper, the bond interface was moved away from the microball wear track on the radial bearing surface to eliminate the large debris generation and the extra cleaning steps and is shown in Fig. 2(b).

The microball bearing raceway design used in this paper is shown in Fig. 3, and Table I shows the parameters and values for the raceway. The parameter h_{race} is used to control the amount of sag within the released rotor. The rotor sag is one of two determinants of the pump gap, i.e., h_2, with the other determinant being the bond layer thickness between the pump manifold and the rotor layer. The width of the raceway is made to be 5 μm wider than the microball diameter to allow for fabrication tolerance, and the width w_2 is made to be wide enough such that the journal edge is outside of the microball wear track. The bond interface was moved 50 μm from the center of the raceway. This value ensures that the bond interface is removed from the microball contact area and wear track area as determined by inspection of the wear track in previous experiments [20].

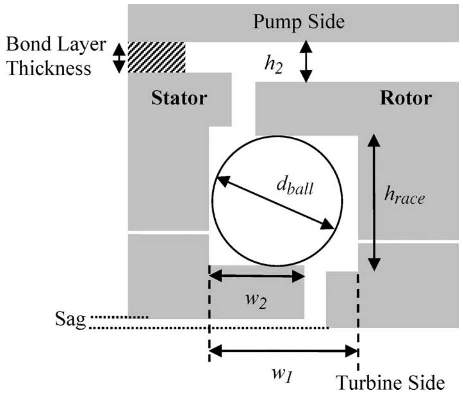

Fig. 3. Schematic of the microball raceway design.

TABLE I
PARAMETERS FOR THE PLANAR-CONTACT BEARING

Bearing Race Parameter	Designed Dimension
d_{ball}	285 µm
h_{race}	290 µm
w_1	290 µm
w_2	30 µm
w_3	190 µm

The operation of this bearing is unidirectional in terms of the applied thrust force. The design of the raceway requires the net thrust force to be in the direction going from the pump side toward the turbine side. This, in turn, requires the pressure on the pump side of the rotor to be greater than the pressure on the turbine side in order for the planar surface of the raceway to contact the microballs. At the same time, the total net thrust force must also overcome the adhesion forces within the pump gap that try to bring the rotor and the pump manifold into contact. The rotor surface can contact the spiral-groove structures and seize the rotor when the net thrust force is in the opposite direction due to the large play in the raceway in that direction.

D. Spiral-Groove Pump

The design for the spiral-groove pump is based on the work published by Muijderman for spiral-groove thrust bearings [21]. Fig. 4 is included to aide in the description of the geometrical variables for the spiral-groove impeller. The performance

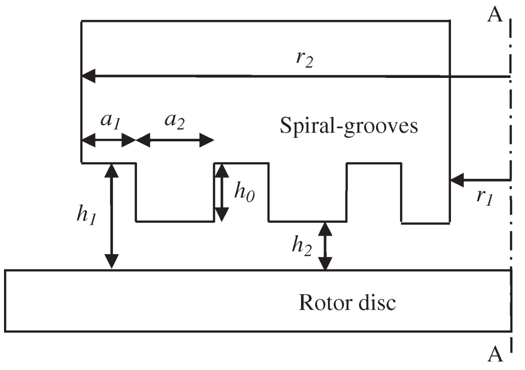

Fig. 4. Diagram illustrating the groove geometry and gap within the spiral-groove viscous pump. The rotational axis is denoted by the A–A′ dashed line.

TABLE II
OPTIMIZED PUMP PARAMETERS

Parameter	Definition	Value
α	Spiral angle	16.6°
H	Gap Ratio (h_2/h_1)	0.29
γ	Groove to spiral width Ratio (a_1/a_2)	1

of the pump in terms of the pressure rise through the pump region follows the analytical equation [21]

$$\Delta p = \frac{3\eta\omega}{h_2^2}\left(r_2^2 - r_1^2\right) g_1(\alpha, H, \gamma) - \frac{6\eta Q(1+\gamma)}{\pi h_1 h_2^2} H_1(\alpha, H, \gamma) \ln\left(\frac{r_2}{r_1}\right) \quad (1)$$

where η is the dynamic viscosity of the working fluid, ω is the rotational speed of the rotor, h_2 and h_1 are the pump gap and the gap between the rotor disc and bottom of the groove structures, respectively, r_2 and r_1 are the outer and the inner radius of the pump spiral grooves, respectively, and Q is the volumetric flow rate of the working fluid. The variables g_1, H, and H_1 are complex geometric parameters based on α (the spiral-groove angle), H (the ratio of h_2/h_1), and γ (the ratio of the groove-to-ridge widths a_2/a_1). Table II shows the optimized values for α, H, and γ that were determined by Muijderman [21] and used to calculate g_1, H, and H_1. The raceway dimensions h and w_1 were chosen to have a 5-μm tolerance built-in in addition to the diameter of the microball (285 μm with a diameter tolerance of 0.25 μm). With this tolerance, the expected sag in the rotor is 5 μm, which is shown in Fig. 3.

From (1), the design of the spiral-groove pump relies heavily on the gap h_2, outer radius r_2, and the range of speeds capable with the microball bearing and turbine structure. From [20], the microball bearing and turbine platform was demonstrated to be reliable and repeatable up to 10 000 r/min. Fabrication tolerances dictate the minimum designed gap size, which is 5 μm. In terms of pressure, the largest outer radius is desired; however, the torque has a much larger dependence on the outer radius [21]

$$Torque = \frac{\pi\eta\omega}{2h_2}\left(r_2^4 - r_1^4\right)\frac{g_2(\alpha, H, \gamma)}{(1+\gamma)} - H_2(\alpha, H, \gamma)\left(r_2^2 - r_1^2\right)\frac{\eta Q}{h_1 h_2}. \quad (2)$$

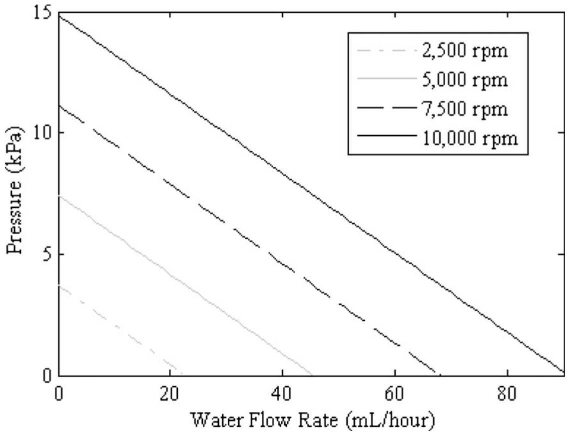

Fig. 5. Turbopump characterization curves describing the relationship between flow rate, pressure rise, and rotational speed for a pump gap of 10 μm.

In this paper, a designed gap of 10 μm was used, with an outer radius of 2.25 mm and an inner radius of 625 μm, to achieve pressures in the range of 7 kPa for flow rates in the range of 10–100 mL/h. The flow rate ranges are suitable for portable power applications using a liquid fuel, and the pressure range is appropriate for a fuel injector (5.2 kPa) that is currently being developed to sufficiently atomize the liquid fuel [22].

Fig. 5 shows the pump curves calculated using (1) for water flow rates up to 90 mL/h and speeds up to 10 000 r/min with a 10-μm gap. These curves demonstrate that our original design point of 5.2 kPa with a 10-mL/h flow rate can be achieved with a rotational speed of 4400 r/min and an estimated torque of 4.6 μN · m required to operate.

III. FABRICATION

The turbopump fabrication is performed in three distinct parts totaling a five-wafer stack (Figs. 6 and 7). The turbine manifold and the bottom side of the rotor layer together make up the radial in-flow microturbine and house the microball bearing. The pump manifold consists of the pump plumbing channels and ports along with the spiral-groove structures that are suspended above the topside rotor surface and comprise the pump region.

A. Rotor

The turbine rotor layer fabrication starts with two double-sided polished 4-in-diameter silicon wafers. The annular raceway is defined in each of the layers along with fluidic holes. On the bottom rotor layer, the raceway is etched to 95 μm, while the opposing wafer is etched to 195 μm [Fig. 6(a)], both using deep reactive ion etching (DRIE) and a patterned AZ9245 thick photoresist masking layer. The different raceway etch depths allow the bond interface between the two layers to be 50 μm from the center of the raceway so that the microball will not contact the interface. After the raceway is etched, journals are patterned using spray-coated AZ4999 photoresist and etched using DRIE [Fig. 6(b)].

The surfaces are cleaned using an O_2 plasma ash, and then, a metal bond layer is deposited by electron beam evaporation on both wafer surfaces to be bonded [Fig. 6(c)]. The bond

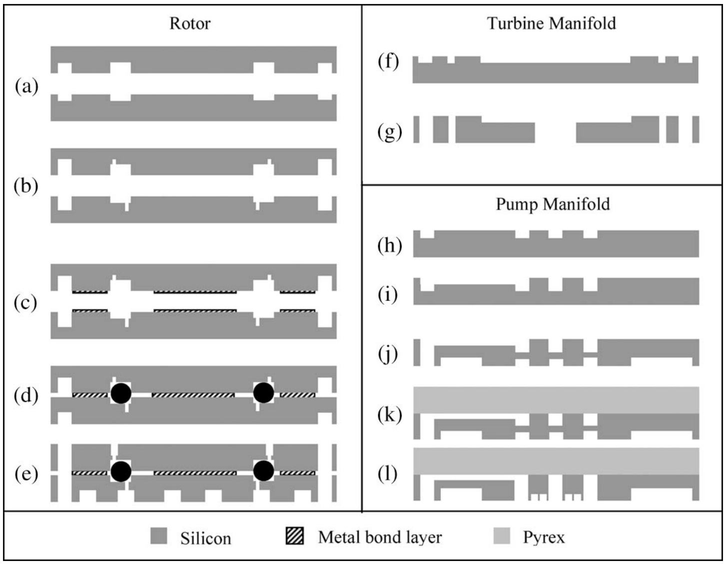

Fig. 6. Microturbopump fabrication process flow.

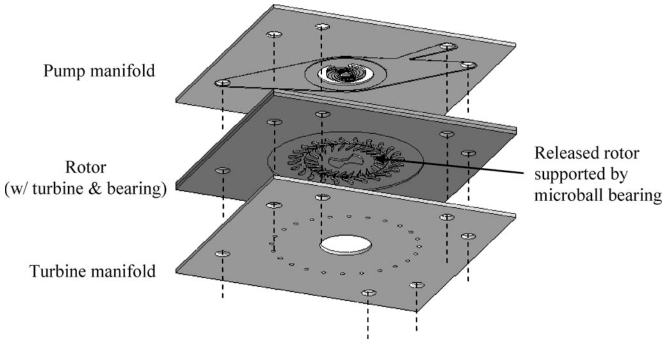

Fig. 7. Schematic showing the distinct layers of the microfabricated turbopump.

layer is composed of Cr (50 nm), Au (50 nm), AuSn (1 μm), and Au (50 nm) stack for eutectic bonding and is patterned by aligning a silicon shadow mask on top during the evaporation deposition. The wafers are diced after metal deposition, and microballs are placed within the silicon raceways in a full compliment fashion, totaling up to 110 microballs. The two layers are aligned using microballs and etched pits with a depth of 145 μm, similar to our previous work [16]–[20]. This enables alignment within 5 μm. The eutectic bond is performed with a temperature of 315 °C and a H_2/N_2 forming gas at 1300 mbar to help break up any oxidation that may have occurred on the surfaces and to maintain a surface free of organics [Fig. 6(d)]. The bond layer does not create a hermetic seal; therefore, no forming gas is trapped inside the raceway.

The final step in the fabrication of the rotor layer is to release the rotor. This is accomplished using a silicon dioxide masking layer and etching the remaining silicon down to the journal extending from the raceway. The silicon dioxide masking layer is patterned prior to dicing the wafers and defines the turbine structures on the bottom side and a release pattern on the topside of the bonded stack [Fig. 6(e)]. In addition to the release patterns, the final through-holes are patterned to complete the fluidic passages. The topside of the rotor is released using a 45-μm-wide annular ring, which is 15 μm wider than the journal to ensure that the complete width of the journal is released. On the same layer, alignment pits (matching the microballs) are provided to align between the rotor layer and pump manifold. In this case, the etch depth to release the rotor from the topside is set to be 145 μm. On the bottom side, the turbine geometry is etched 200 μm to form the turbine structures while, at the same time, releasing the rotor.

B. Turbine Manifold

The turbine manifold is fabricated in a 4-in-diameter double-sided polished silicon wafer using two DRIE etching steps each having a patterned AZ9245 thick photoresist masking layer. The first step [Fig. 6(f)] patterns the fluidic holes and a cavity to provide sufficient clearance for the turbine blades. The normal force on the turbine rotor causes the rotor to sag into the cavity during operation. The depth of the cavity is chosen such that the clearance above the turbine blades is less than 20% of the 200-μm blade height. This is done to minimize tip clearance flow while simultaneously allowing sufficient space for the bearing surfaces to wear without the rotor blades contacting the manifold. The second DRIE step completes the through etches from the backside for the turbine exhaust and fluidic ports [Fig. 6(g)].

C. Pump Manifold

The pump manifold is composed of a 4-in-diameter double-sided polished silicon wafer with channels on the topside and pumping structures on the bottom side [Fig. 6(h)–(l)]. The pump inlet, pump outlet, and fluidic port through-holes are started on the topside of the 4-in silicon wafer [Fig. 6(h)] using DRIE and an AZ9245 thick photoresist masking layer. Next, the fluidic channels are patterned into the silicon to a depth of 200 μm using DRIE and a 1-μm-thick silicon dioxide masking layer deposited using plasma-enhanced chemical vapor deposition [Fig. 6(i)]. The nitrogen balance channels and fluidic through-holes are then patterned on the backside of the

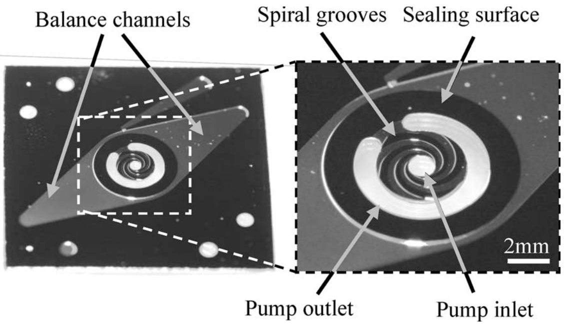

Fig. 8. Optical image of the spiral-groove pump manifold showing the grooves and sealing surface.

wafer using DRIE and an AZ9245 photoresist masking layer [Fig. 6(j)]. A Pyrex wafer is attached to the topside of the wafer using anodic bonding, capping off the pump inlet and outlet channels [Fig. 6(k)]. The final DRIE is performed to define the pump spiral grooves [Fig. 6(l)] using a 1-μm-thick silicon dioxide masking layer. This step is not performed until the sag of the rotor is measured and the required groove depth is determined to satisfy the optimized ratio $H = 0.29$ from [21].

The pump gap is dictated by both the bond layer thickness used to bond the pump manifold to the rotor layer and the final sag exhibited by the rotor. The average rotor sag for bonded rotors was measured using an optical profilometer to be 5 ± 1 μm. The bonding layer thickness is determined in the final assembly step described in the following section. A single pump manifold was used for the devices in this paper and had a spiral-groove depth of 27.5 μm, which was optimized for a pump gap of 11 μm (Fig. 8).

D. Turbopump Layer Assembly

The turbopump layers shown in Fig. 7 are assembled together at the die level. The pump manifold layer is first bonded to the rotor layer via photoresist. Photoresist was chosen as a temporary bond layer to allow the pump gap to be easily modified and was deposited by spraying the photoresist, using a Suss Microtec Altaspray system, through a silicon shadow mask. The photoresist layer covered an approximate surface area of 450 mm^2. Photoresist bonding was performed on a hotplate at 110 °C for 3 min with a 100-g weight placed on top of the stack. Knowing the final thickness of the photoresist bond layer is crucial in determining the fabricated pump gap. The sprayed-on photoresist thickness was measured on a separate sample using the same curing temperature and time, but without compression. In these measurements, the thickness variation across the die was ± 0.5 μm. The thickness of the bonded photoresist is not readily measured but is believed to shrink significantly during the baking procedure due to compression and solvent evaporation. The original photoresist thickness used in this paper was 10 μm so that the resulting minimum pump gap after photoresist shrinkage would be the designed 10 μm. In this case, the photoresist thickness is believed to be anywhere from 5 to 10.5 μm, and thus, the total pump gap, including the rotor sag, is estimated to be between 9 and 17.5 μm.

Fig. 9. Optical image showing an assembled turbopump device.

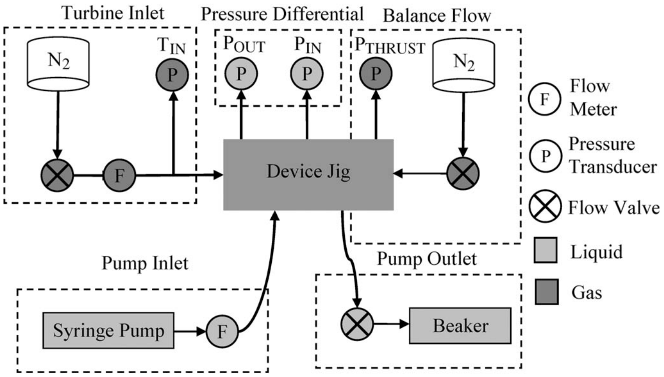

Fig. 10. Diagram of the turbopump experimental setup.

Before bonding the turbine manifold to the rotor stack, tubulations were attached for fluidic connection using epoxy. The turbine manifold is assembled with the rotor/pump stack by clamping using a lid in the device jig and the jig cavity to align the layers. Fig. 9 shows an assembled turbopump device, which has a total volume of 1.5 cm^3, including the large through-holes at the periphery of the device. These through-holes were designed to simplify the experimental characterization and could be removed for practical implementation of an integrated device. Not considering the added volume for these fluidic paths, the device volume is 0.8 cm^3.

IV. TESTING AND RESULTS

A. Experimental Apparatus

The experimental apparatus used to characterize the microturbine and turbopump is shown in Fig. 10, and an image of the device fixture is shown in Fig. 11. The pressure, liquid, and gas handling ports correspond to the through-holes on the turbopump device. Five key areas are outlined: 1) turbine inlet; 2) pump inlet; 3) thrust balance; 4) pump pressure differential; and 5) pump outlet.

Control of the turbine is achieved using pressurized nitrogen with an inline manual control valve and an Omega FMA series flow meter (0–50 slm). The pressure entering the turbine inlet is monitored using an Omega PX480A-060GV pressure transducer. The flow rate of the turbine is controlled via the manual valve and logged with the turbine inlet pressure. The turbine exit is exhausted to ambient.

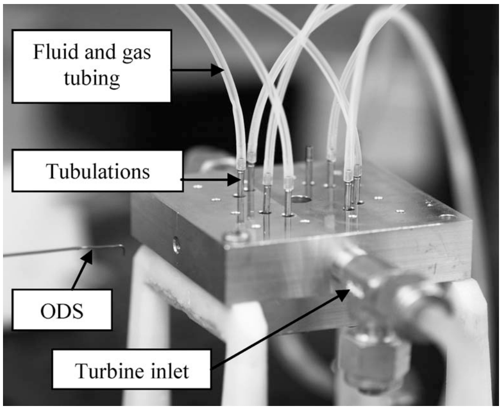

Fig. 11. Image of the device fixture. The device is packaged inside of the fixture, and the tubulations can be seen that attached to the device.

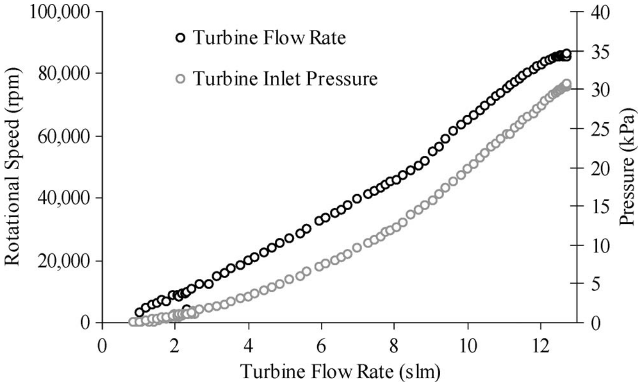

Fig. 12. Turbine characterization curves exhibiting up to 87 000 r/min in air and 30-kPa turbine inlet pressure.

The balance flow is controlled via a manual control valve in line with the device and nitrogen source. An Omega PX181-015G5V pressure transducer monitors the balance pressure at the periphery of the rotor. The balance pressure is maintained above the pump outlet pressure to prevent liquid from entering the bearing. This is necessary to ensure that the microball bearings remain dry during operation of the turbopump.

The working liquid is fed into the pump inlet using a syringe pump with a 1-μm inline filter. The syringe pump was used to prime the turbopump and to maintain a fixed flow rate during the experiments. The liquid exiting at the pump outlet is fed to a beaker. The liquid pressure at the pump outlet is controlled using a manual flow valve. The pressure rise across the pump is measured using two Omega PX480A-001GV pressure transducers (0.3% full scale accuracy) placed at the pump inlet and outlet pressure taps.

The optical displacement sensor (ODS) shown in Fig. 11 is used to detect the speed of rotation using the measurement geometry at the center of the turbine rotor. A D6 ODS from Philtec, Inc., is connected in line with a 200-kHz voltage amplifier and fed to a data acquisition card along with all of the voltage signals from the pressure transducers and flow meter. A PC running NI LabVIEW software is used to monitor all pressures along with the turbine flow rate and rotor speed. All pressure transducers were calibrated to zero using the logged data at ambient conditions so that all pressure measurements are relative to atmospheric pressure.

B. *Microturbine and Bearing Characterization*

The microturbine and microball bearing performance and robustness were characterized without the pump manifold using a high-speed/high-load test. The performance before and after the pump manifold is assembled was also characterized at 10 000 r/min, which was the upper design speed for the turbopump. Before the pump manifold was assembled to the rotor stack, testing was performed using only the rotor layer and the turbine manifold. The topside of the rotor was sealed by a gasket (in place of the pump manifold), and an o-ring having a thickness of 1.6 mm was used to create a large air gap and to ensure that air drag is negligible.

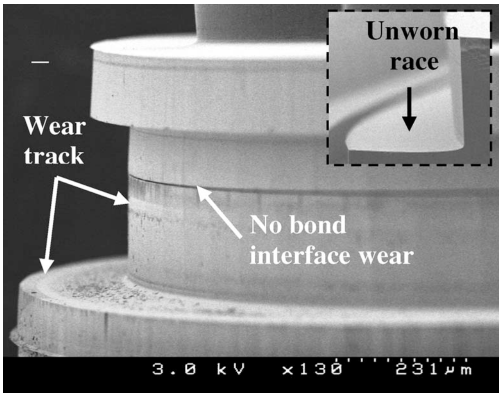

Fig. 13. SEM image showing the worn raceway after a maximum speed of 87 000 r/min, exhibiting minimal wear. An image of an unworn surface is shown in the inset of the image.

A high-speed and high-loading test was performed by increasing the turbine inlet flow to the maximum pressure of the nitrogen supply. This allowed a maximum flow rate of 13 slm to pass through the turbine. During this test, the turbine flow also accesses the sealed topside of the rotor through the bearing journals and pressurizes the cavity. The pressure exerted on the rotor surface created an approximate thrust force of 2.2 N. This force was calculated by integrating the measured pressures across the top and bottom surfaces of the rotor. The pressure between each measurement was assumed to drop linearly; therefore, the calculated thrust force is an approximation. A high speed up to 87 000 r/min was achieved as shown in Fig. 12; however, device performance afterward was decreased.

After the test was performed, the device was disassembled to inspect the microball raceway and determine the amount of wear. Scanning electron microscopy (SEM) inspection shows minimal raceway wear in Fig. 13 after approximately 100 000 revolutions and maximum rotational speed of 87 000 r/min. The wear track was measured to be less than 100 nm deep using an optical profilometer. An accurate measurement is difficult due to the surface roughness and curvature of the DRIE surface where the raceway wear appears to be a smoothing of the surface roughness peaks rather than wearing of the underlying silicon. The reason for decreased performance after reaching the maximum was not readily evident but is believed to be due to fracturing of thin sections of the raceway due to the extreme thrust force. Other devices have been routinely

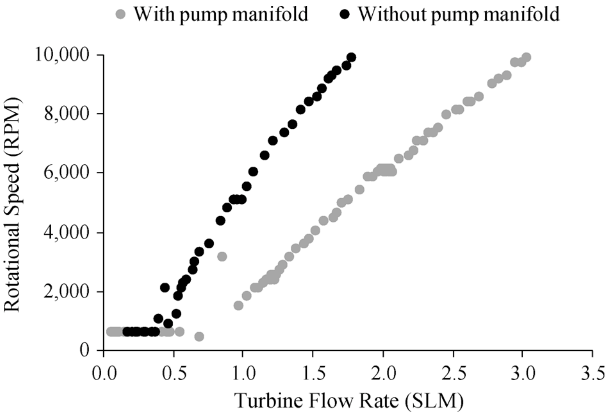

Fig. 14. Turbine characterization up to 10 000 r/min in air before and after packaging the pump manifold layer.

operated at speeds greater than 50 000 r/min without significant performance decreases. The observed thrust force of 2.2 N is ten times higher than the forces on the rotor during pumping and, when combined with the significantly higher rotor speed, is expected to exhibit larger amount of wearing.

The operation of the turbine was also characterized before and after the pump manifold was attached to generate a baseline turbine performance and to ensure that the assembly procedure does not adversely affect the turbine operation. The observed viscous drag and startup friction is expected to be greater when the pump manifold is attached due to the small gap between the pump manifold and the rotor. This was seen in the characterization results shown in Fig. 14 by the increased turbine flow to spin the rotor at the same speed as without the pump manifold. This characterization verifies proper turbine performance and was performed throughout the experiments to monitor the bearing operation.

The modified planar-contact bearing developed in this paper was able to achieve more than 3.5 million revolutions with an average speed of 10 000 r/min without any decrease in turbine performance and no cleaning. This continuous operation, together with rotational speeds up to 87 000 r/min, demonstrates a notable improvement over previous work where the bond interface between the two rotor layers generated substantial debris and limited performance.

C. Turbopump Characterization

The turbopump is started by introducing the liquid within the pumping structures before spinning the rotor. The pump outlet pressure is monitored so that the balance pressure at the periphery can be adjusted, thereby maintaining a seal between the liquid and air. For most experiments, the initial flow rate was set by the syringe pump to be 60 mL/h, and the balance pressure was maintained at 6.2 kPa with a 3.2-kPa pump outlet pressure as shown in Fig. 15. Without the rotor spinning (before time t_1), the pressure at the pump inlet is larger than the pressure at the pump outlet because the syringe pump is providing a pressure-driven flow. In this case, energy is lost through the static pumping structures, and the pressure rise through the pump region is negative. The turbopump is not considered to be pumping until the pressure rise through the pump is positive. This is when the pump is increasing the energy of the fluid through the pump region rather than decreasing it.

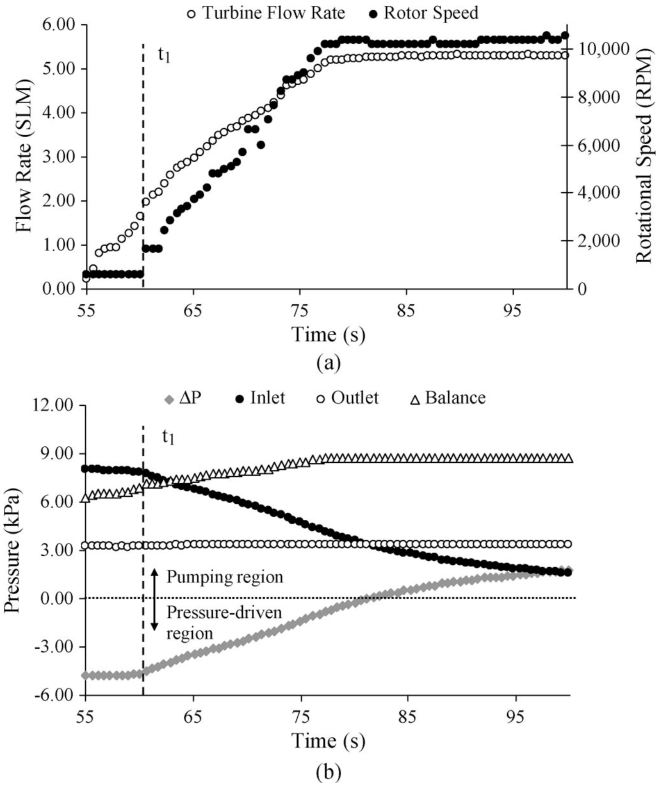

Fig. 15. Start-up procedure for the turbopump showing (a) turbine parameters and (b) pumping parameters.

The pump was started at time t_1 (Fig. 15) by providing flow through the turbine manifold. The flow rate through the turbine was increased until the speed reached 10 000 r/min. At this speed and liquid flow rate, the pressure rise through the pump settles to +2.2 kPa, meaning that the turbopump is considered to be pumping.

Pump operation was characterized using a device having a gap estimated to a range between 9 and 17.5 μm. During testing, the pump outlet was kept elevated at 3.5 kPa to ensure that the normal force exerted on the rotor was enough to be greater than the adhesion forces at all rotor speeds and pump pressures. The flow rate was varied from 10 to 80 mL/h using the syringe pump. The pressure rise through the pump was measured across the range of flow rates for rotor speeds of 5000, 7500, and 10 000 r/min. The maximum pressure rise of 8.2 kPa was observed with a rotor speed of 10 000 r/min and a liquid flow rate of 10 mL/h.

The experimental data were compared to (1) by assuming a range of possible pump gaps. It is difficult to know exactly the gap due to photoresist shrinkage during the bonding process and the nonuniformity of the photoresist and rotor sag. Fig. 16 shows the pump curve for 10 000 r/min and a pump gap ranging between 10 and 16 μm corresponding to the possible range of pump gaps. The experimental data fit well to a pump gap corresponding to 12 μm. The analytical lines that correspond to the pump gap of 12 μm are shown in Fig. 17 along with the experimental results for the three rotational speeds, which show good agreement.

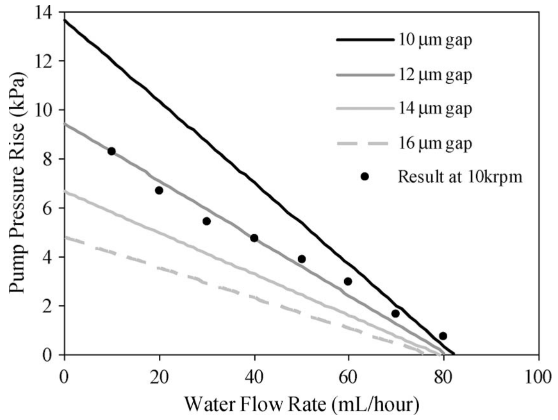

Fig. 16. Experimental versus analytical comparison for 10 000 r/min.

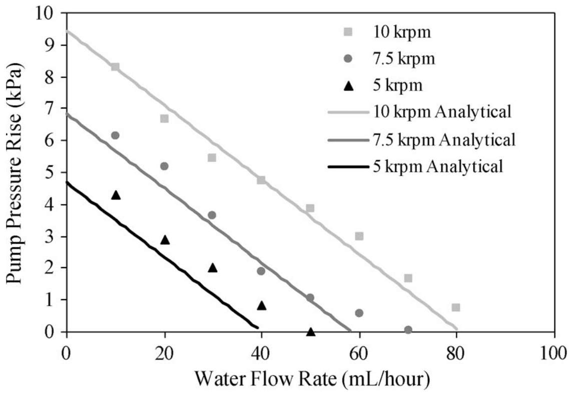

Fig. 17. Experimental pump characterization curves plotted with curves based on (1) using a 12-μm pump gap.

V. Discussion

The air turbine in the turbopump developed is envisioned to be replaced with an electrically driven micromotor to enable a controlled fuel delivery in power generation applications. For this purpose, rotational speeds around the 10 000-r/min mark were investigated. Integration with an electronically driven micromotor will enable precision control and a broad range of applications beyond just the PowerMEMS applications being sought after in our effort. Ongoing development of a variable capacitance micromotor has shown the potential to operate in the range of 10 000 r/min [23]. Our results have shown the microball bearing mechanism to be stable in the 10 000-r/min range; however, higher speed operation may be possible. At higher rotational speeds, the pump region can be made smaller, thereby drastically reducing the torque required to operate the pump for the same flow rates and pressures.

The low wear within the bearings, even the demonstrated low wear for the high-speed operation at 87 000 r/min, suggests a long lifetime, but further experiments are required to quantitatively predict the wear and lifetimes of these devices. A first step to improve both the friction and lifetime is to investigate solid-film lubricants to be applied on the silicon raceway surface. This will allow a hybrid bearing mechanism in which the ball material properties and raceway material properties may be matched better in terms of optimum Young's modulus and hardness values [24], [25].

As shown from the friction characterization in [20], it will be critical to control the normal force to reduce the friction. Normal force control is also critical for the spiral-groove viscous pump demonstrated in this paper as it ensures the proper thrust direction in the rotor and maintains the pump gap. By controlling a micromotor's pull on the rotor, the bearing mechanism can be flipped, and a smaller pump gap maintained through the electrically induced normal force rather than the pneumatic balance feed and pump inlet pressure control used in this paper. Smaller pump gaps were investigated using the latter approach; however, continuous pumping could not be achieved. Adhesion forces become more dominant in devices with smaller gaps and require a larger separation pressure force across the pump region. At sufficiently low rotor normal forces, the rotor is believed to lift off the microball raceway surface and close the gap between the top rotor surface and the spiral grooves on the pump manifold. This causes an increase in the viscous loss within the gap, slowing the rotor and, in the case of smaller gap configurations, seizing the turbine. An alternative design of the pump manifold, rotor orientation, and air turbine mechanism, which accounts for the adhesion forces, may be developed to enable smaller pump gaps and increased performance.

The design of the turbopump and the experimental platform developed allow many configurations of viscous pump geometries to be utilized on the pump manifold layer using a single rotor. The analytical model used to design the spiral-groove structures and gap assumed a linear pressure distribution in the spiral-groove region [21]. In addition, this paper did not take into account the effect of the spiral-groove ends where the pressure distribution cannot be assumed linear or microchannel flow effects such as the viscous dissipation and entrance effects as described by Koo and Kleinstreuer [26]. These unaccounted effects may be able to describe the small discrepancy between the experimental data and (1) that is shown in Fig. 17. The turbopump platform can be used to investigate the fluid dynamics of the spiral-groove design and can serve as a platform to optimize the critical spiral-groove geometries such as α, H, and γ in (1). Furthermore, the platform allows for many types of rotary viscous pumps to be investigated.

VI. Summary and Conclusion

In summary, the first pumping action using a turbopump supported by microball bearings was demonstrated in this paper, highlighting the potential of this technology for a variety of liquid pumping applications. A turbopump was created by integrating together a radial in-flow microturbine actuation mechanism, a modified microball bearing support mechanism, and a spiral-groove pump. The microturbine was characterized up to 10 000 r/min after initial rotor fabrication as well as after being assembled into a turbopump and found to be repeatable with revolutions greater than 3.5 million without cleaning. The turbine performance was observed to improve with the modified planar-contact bearing design when compared with a previous microturbine that was used to study bearing friction. Furthermore, high-speed operation of the turbine and microball bearing was demonstrated with rotational speeds up to 87 000 r/min. Continued work focuses on hard coatings to reduce the friction between the raceway and microball [23], [24] and, therefore, further increase the potential speeds.

A microfabricated turbopump was characterized at rotational speeds ranging from 5000 to 10 000 r/min and achieved flow rates from 10 to 80 mL/h, reaching a maximum pressure rise of 8.2 kPa. These flow rate and pressure ranges meet the requirements for portable power applications and upstream components currently under development. The experimental curves were compared to the analytical equation for pressure rise and found to fit well with a 12-μm pump gap.

The design and development of robust methods for encapsulated microball bearings, microturbines, and pumping structures have culminated in the successful demonstration of a microturbopump. Not only do the components developed allow for liquid pumping but also alternative applications are envisioned. The microball bearing platform developed and characterized enables other MEMS applications to be effectively designed and incorporated into numerous rotary applications. Lastly, the bearing mechanism and pumping technology can be thoroughly investigated and optimized using the platform described.

ACKNOWLEDGMENT

The authors would like to thank the Army Research Laboratory Specialty Electronic Materials and Sensors Cleanroom personnel for their support in the fabrication of the devices. The authors would also like to thank C. Rorick for his assistance in developing the turbopump test-stand.

REFERENCES

[1] A. H. Epstein, “Millimeter-scale, MEMS gas turbine engines,” presented at the ASME Turbo Expo., Atlanta, GA, Jun., 2003, Paper GT-2003-38866.

[2] K. Isomura, M. Murayama, S. Teramoto, K. Hikichi, Y. Endo, S. Togo, and S. Tanaka, “Experimental verification of the feasibility of a 100 W class micro-scale gas turbine at an impeller diameter of 10 mm,” *J. Micromech. Microeng.*, vol. 16, no. 9, pp. S254–S261, Sep. 2006.

[3] J. Peirs, D. Reynaerts, and F. Verplaetsen, “A microturbine for electric power generation,” *Sens. Actuators A, Phys.*, vol. 113, no. 1, pp. 86–93, Jun. 2004.

[4] L. G. Fréchette, C. Lee, S. Arslan, and Y.-C. Liu, “Design of a microfabricated Rankine cycle steam turbine for power generation,” in *Proc. ASME Int. Mech. Eng. Congr. Micro-Electromech. Syst. Division*, 2003, vol. 5, pp. 335–344.

[5] D. C. Walther and A. P. Pisano, “MEMS rotary engine power system: Project overview and recent research results,” in *Proc. 4th Int. Symp. MEMS Nanotechnol.*, 2003, pp. 227–234.

[6] X. Zhang, D. Zheng, T. Wang, C. Chen, J. Cao, J. Yan, W. Wang, J. Liu, H. Liu, J. Tian, X. Li, H. Yang, and B. Xia, “A preliminary study of a miniature planar 6-cell PEMFC stack combined with a small hydrogen storage canister,” *J. Power Sources*, vol. 166, no. 2, pp. 441–444, Apr. 2007.

[7] S. K. Kamarudin, W. R. W. Daud, S. L. Ho, and U. A. Hasran, “Overview on the challenges and developments of micro-direct methanol fuel cells (DMFC),” *J. Power Sources*, vol. 163, no. 2, pp. 743–754, Jan. 2007.

[8] N.-T. Nguyen, X. Huang, and T. K. Chuan, “MEMS-micropumps: A review,” *Trans. ASME, J. Fluids Eng.*, vol. 124, no. 2, pp. 384–392, Jun. 2002.

[9] D. J. Laser and J. G. Santiago, “A review of micropumps,” *J. Micromech. Microeng.*, vol. 14, no. 6, pp. R35–R64, Apr. 2004.

[10] D. Blanchard, P. Ligrani, and B. Gale, “Miniature single-disk viscous pump (single-DVP), performance characterization,” *Trans. ASME, J. Fluids Eng.*, vol. 128, no. 3, pp. 602–610, May 2006.

[11] A. Deux, “Design of a silicon microfabricated rocket engine turbopump,” Ph.D. dissertation, MIT, Cambridge, MA, 2001.

[12] C. Lee, M. Liamini, and L. Fréchette, “Design, fabrication, and characterization of a microturbopump for a rankine cycle micro power generator,” in *Proc. IEEE Int. Conf. Solid-State Sens., Actuators, Microsyst.*, Hilton Head Island, SC, Jun. 4–8, 2006, pp. 276–279.

[13] R. Ghodssi, D. D. Denton, A. A. Seireg, and B. Howland, “Rolling friction in a linear microactuator,” *J. Vac. Sci. Technol. A, Vac. Surf. Films*, vol. 11, no. 4, pp. 803–807, Jul. 1993.

[14] T.-W. Lin, A. Modafe, B. Shapiro, and R. Ghodssi, “Characterization of dynamic friction in MEMS-based microball bearings,” *IEEE Trans. Instrum. Meas.*, vol. 53, no. 3, pp. 839–846, Jun. 2004.

[15] X. Tan, A. Modafe, and R. Ghodssi, “Measurement and modeling of dynamic rolling friction in linear microball bearings,” *Trans. ASME, J. Dyn. Syst. Meas. Control*, vol. 128, no. 4, pp. 891–898, Dec. 2006.

[16] C. M. Waits, B. Geil, and R. Ghodssi, “Encapsulated ball bearings for rotary micro machines,” *J. Micromech. Microeng.*, vol. 17, no. 9, pp. S224–S229, Aug. 2007.

[17] C. M. Waits, N. Jankowski, B. Geil, and R. Ghodssi, “MEMS rotary actuator using an integrated ball bearing and air turbine,” in *Proc. 14th Int. Conf. Solid-State Sens., Microsyst. Transducers*, Lyon, France, Jun. 10–14, 2007, pp. 1131–1134.

[18] M. McCarthy, C. M. Waits, and R. Ghodssi, “Development of a hybrid gas/ball bearing support mechanism for microturbomachinery,” in *Proc. 7th Int. Workshop Micro Nanotechnol. Power Generation Energy Conversion Appl. Power MEMS*, Frieburg, Germany, Nov. 28–29, 2007, pp. 241–244.

[19] M. McCarthy, C. M. Waits, and R. Ghodssi, “Dynamic friction and microturbine performance using a planar-contact encapsulated microball bearing,” in *Proc. IEEE Int. Conf. Solid-State Sens., Actuators, Microsyst.*, Hilton Head Island, SC, Jun. 1–5, 2008, pp. 170–173.

[20] M. McCarthy, C. M. Waits, and R. Ghodssi, “Dynamic friction and wear in a planar-contact encapsulated microball bearing using an integrated microturbine,” in *J. Microelectromech. Syst.*, Apr. 2009, vol. 18, no. 2, pp. 263–273.

[21] E. A. Muijderman, *Spiral Groove Bearings*, vol. 198. Eindhoven, The Netherlands: N.V. Philips’ Gloeilampenfabrieken, 1966.

[22] C. M. Waits, B. Morgan, W. Deng, N. R. Jankowski, A. Gomez, and B. Geil, “Microfabricated high density multiplexed electrospray,” in *Proc. IEEE Int. Conf. Solid-State Sens., Actuators, Microsyst.*, Hilton Head Island, SC, Jun. 1–5, 2008.

[23] M. McCarthy, C. M. Waits, M. I. Beyaz, and R. Ghodssi, “A rotary microactuator supported on encapsulated microball bearings using an electro-pneumatic thrust balance,” in *Proc. 22nd IEEE Int. Conf. MEMS*, Sorrento, Italy, Jan. 15–29, 2009, pp. 1095–1098.

[24] B. Hanrahan, M. McCarthy, C. Zorman, and R. Ghodssi, “Wear in MEMS-based microball bearings,” in *Proc. Amer. Vac. Soc. 54th Int. Symp.*, Seattle, WA, Oct. 14–19, 2007.

[25] M. McCarthy, B. Hanrahan, C. Zorman, and R. Ghodssi, “Rolling friction in MEMS ball bearings: The effects of loading and solid film lubrication,” in *Proc. STLE/ASME Int. Joint Tribology Conf.*, San Diego, CA, Oct. 22–24, 2007.

[26] J. Koo and C. Kleinstreuer, “Liquid flow in microchannels: Experimental observations and computational analyses of microfluidics effects,” *J. Micromech. Microeng.*, vol. 13, no. 5, pp. 568–579, May 2003.

Christopher Mike Waits (S’01) received the B.S. degree in physics from Salisbury University, Salisbury, MD, in 2000 and the M.S. and Ph.D. degrees in electrical engineering from the University of Maryland, College Park, in 2003 and 2008, respectively.

Since 2004, he has been an Electronics Engineer with the Sensors and Electron Devices Directorate, U.S. Army Research Laboratory, Adelphi, MD. His main research interests include microelectromechanical systems (MEMS) components and systems focused on power and energy generation and conversion (PowerMEMS), MEMS tribology and bearing mechanisms, and new microfabrication techniques.

Dr. Waits was the recipient of the Physics Excellence Award from Salisbury University in 2000, the Graduate Assistance in Areas of National Need (GAAN) Fellowship from 2001 to 2003, and the Department of the Army Research and Development Achievement Award for Technical Excellence in 2007.

Matthew McCarthy received the B.S. degree in aerospace engineering from Syracuse University, Syracuse, NY, in 2002 and the M.S. and Ph.D. degrees in mechanical engineering from Columbia University, New York, NY, in 2004 and 2006, respectively.

From 2007 to 2008, he was a Postdoctoral Research Associate with the MEMS Sensors and Actuators Laboratory, Department of Electrical and Computer Engineering, Institute for Systems Research, University of Maryland, College Park. He is currently a Postdoctoral Associate with the Department of Mechanical Engineering, Massachusetts Institute of Technology, Cambridge. His research interests are in the field of multiscale thermal, fluidic, and energy technologies. His current efforts are focused on the development of micro- and nanostructures for energy storage devices, sensors and actuators, and compact cooling systems.

Reza Ghodssi (S'92–M'96) received the B.Sc., M.Sc., and Ph.D. degrees from the Electrical Engineering Department, University of Wisconsin, Madison, in 1990, 1992, and 1996, respectiveley.

He is currently the Herbert Rabin Distinguished Professor, the Director of the Institute for Systems Research, and the Director of the MEMS Sensors and Actuators Laboratory, Department of Electrical and Computer Engineering, University of Maryland (UMD), College Park. He is also currently with the Fischell Department of Bioengineering, the Maryland NanoCenter, the University of Maryland Energy Research Center, and the Materials Science and Engineering Department, UMD. His research interests are in the design and development of microfabrication technologies and their applications to micro/nanodevices and systems for chemical and biological sensing, small-scale energy conversion, and harvesting. He has over 70 scholarly publications. He is the Coeditor of the *Handbook of MEMS Materials and Processes* (to be published in 2009) and is an Associate Editor for the *Journal of Micorelectromechanical Systems* and *Biomedical Microdevices*.

Dr. Ghodssi is a member of the American Vacuum Society, the Materials Research Society, the American Society for Engineering Education, and the American Association for the Advancement of Science. He is the Chair of the 9th International Workshop on Micro and Nanotechnology for Power Generation and Energy Conversion Applications, also known as "PowerMEMS 2009" and the Americas Technical Program Committee Chair of the IEEE Sensors 2010 Conference. He is the Cofounder of MEMS Alliance in the greater Washington area. He was the recipient of the 2001 UMD George Corcoran Award, the 2002 National Science Foundation CAREER Award, and the 2003 UMD Outstanding Systems Engineering Faculty Award.